Limnol. Oceanogr., 50(6), 2005, 1945–1959

Nitrogen processing in a tidal freshwater marsh: A whole-ecosystem ^{15}N labeling study

Britta Gribsholt[1] *and Henricus T. S. Boschker*
Netherlands Institute of Ecology (NIOO-KNAW), Centre for Estuarine and Marine Ecology, Korringaweg 7, 4401 NT Yerseke, The Netherlands

Eric Struyf
University of Antwerp, Department of Biology, Ecosystem Management Research Group, Universiteitsplein 1, B-2610 Wilrijk, Belgium

Maria Andersson and Anton Tramper
Netherlands Institute of Ecology (NIOO-KNAW), Centre for Estuarine and Marine Ecology, Korringaweg 7, 4401 NT Yerseke, The Netherlands

Loreto De Brabandere
Vrije Universiteit Brussel, Department of Analytical and Environmental Chemistry, Pleinlaan 2, B-1050 Brussel, Belgium

Stefan van Damme
University of Antwerp, Department of Biology, Ecosystem Management Research Group, Universiteitsplein 1, B-2610 Wilrijk, Belgium

Natacha Brion
Vrije Universiteit Brussel, Department of Analytical and Environmental Chemistry, Pleinlaan 2, B-1050 Brussel, Belgium

Patrick Meire
University of Antwerp, Department of Biology, Ecosystem Management Research Group, Universiteitsplein 1, B-2610 Wilrijk, Belgium

Frank Dehairs
Vrije Universiteit Brussel, Department of Analytical and Environmental Chemistry, Pleinlaan 2, B-1050 Brussel, Belgium

Jack J. Middelburg and Carlo H. R. Heip
Netherlands Institute of Ecology (NIOO-KNAW), Centre for Estuarine and Marine Ecology, Korringaweg 7, 4401 NT Yerseke, The Netherlands

Abstract

We quantified the fate and transport of watershed-derived ammonium in a tidal freshwater marsh fringing the nutrient-rich Scheldt River in a whole-ecosystem ^{15}N labeling experiment. $^{15}N\text{-}NH_4^+$ was added to the floodwater entering a 3,477 m^2 tidal marsh area, and marsh ammonium processing and retention were traced in six subsequent tide cycles. We present data for the water phase components of the marsh system, in which changes in concentration and isotopic enrichment of NO_3^-, NO_2^-, N_2O, N_2, NH_4^+, and suspended particulate nitrogen (SPN) were measured in concert with a mass balance study. Simultaneous addition of a conservative tracer (NaBr) confirmed that tracer was evenly distributed, and the Br^- budget was almost closed (115% recovery). All analyzed dissolved and suspended N pools were labeled, and 31% of added $^{15}N\text{-}NH_4^+$ was retained or transformed. Nitrate was the most important pool for ^{15}N, with nitrification accounting for 30% of ^{15}N-transformation. In situ whole-ecosystem nitrification rates were four to nine times higher than those in the water column alone, implying a crucial role for the large reactive marsh surface area in N-transformation. Under conditions of low oxygen concentrations and high ammonium availability, nitrifiers produced N_2O. Our results show that tidal freshwater marshes function not only as nutrient sinks but also as nutrient transformers.

Estuaries are well known to modify and attenuate nitrogen (N) transfer from rivers to the coastal sea (Billen et al. 1991), and tidal marshes have been reported to play a major role in nitrogen retention (Bowden 1987; Howarth et al. 1996; Cai et al. 2000). Marshes have high surface areas of sediment and biofilms in contact with the water, promoting processes that may change nitrogen speciation and may remove dissolved inorganic and organic nitrogen and enhance deposition of particulate nitrogen (Dame et al. 1996; Merrill

[1] Corresponding author (B.Gribsholt@nioo.knaw.nl).

Acknowledgments

We thank the staff at the NIOO-CEME analytical laboratory for their assistance. This research is part of the Flemish–Dutch co-operation on Coastal Research (VLANEZO) (832.11.004; The role of freshwater marshes in the retention and transformation of nitrogen in estuaries, a whole-ecosystem labeling study), funded by the Flemish and Dutch Science Foundations FWO-NWO. This is NIOO publication 3539.

and Cornwell 2000). There is considerable interest in exploiting the nitrogen 'filtration' capacity of wetland ecosystems in order to improve estuarine and coastal marine water quality. However, despite the widely held belief that wetland systems are important nutrient sinks, the literature regarding the influence of tidal freshwater wetlands on water quality is remarkably small (Merrill and Cornwell 2000). There is still much uncertainty about the underlying mechanisms and controls of nitrogen retention in marsh ecosystems, thus hindering their potential use and effective management for improvement of water quality.

The importance of freshwater marshes to the estuarine nitrogen budget is most often estimated with a mass-balance approach. This technique, however, is subject to considerable error and yields little information regarding the role and spatial and temporal distribution of the underlying processes. Use of stable isotope tracers to track N through aquatic ecosystems in situ is a relatively recent technique and has provided increased understanding of N processing in groundwater plumes (Tobias et al. 2001), lakes (Kling 1994), streams (Peterson et al. 1997; Tank et al. 2000; Hamilton et al. 2001), and small estuaries (Holmes et al. 2000; Hughes et al. 2000; Tobias et al. 2003). Here we present the results of a whole-ecosystem $^{15}NH_4^+$ tracer addition experiment to quantify the fate and transport of watershed-derived ammonium through a tidal freshwater marsh system. Combined with a mass-balance study, this approach allows a simultaneous examination of transport and processing of nitrogen in an intact ecosystem, something that is impossible to achieve in traditional bottle, enclosure, or mesocosm experiments (Schindler 1998; Holmes et al. 2000). Furthermore, this technique allows us to estimate whole-ecosystem nitrogen uptake and transformation without the confounding effects of altering floodwater N concentrations significantly.

The whole-ecosystem ^{15}N labeling experiment was conducted in a tidal freshwater marsh fringing the nutrient-rich Scheldt River. Although many tidal marshes of the Scheldt basin have been reduced to very small size today (mainly by embankment for polder reclamation) (Desender and Maelfait 1999), they are still a prominent feature of the Scheldt, and the surfaces of the ~4.5 km^2 of tidal freshwater marshes could represent important potential N sinks. Yet the importance of these marshes as nutrient sinks within the estuary remains largely unassessed. In this article we present results of the ^{15}N tracing through the water-phase components of the marsh system. ^{15}N tracer incorporation into sediments, macrophytes, and higher trophic levels (pelagic and benthic) will be described in detail in a separate article. Our results show that the marsh is an intense site for nitrification and that nutrient-rich tidal freshwater marshes function not only as nutrient sinks but also as nutrient transformers.

Materials and methods

Study area—The study was conducted in a tidal freshwater marsh fringing the Scheldt and Durme Rivers at Tielrode (51°06″N, 4°10″E), Belgium, where the small tributary Durme flows into the Scheldt approximately 100 km from the mouth of the Scheldt estuary. Because of the funnel-shaped morphology of the Scheldt estuary, the tidal range (5.3 m) and turbidity are here at their maxima. A detailed description of the hydrodynamic features and basin morphology of the Scheldt estuary is given by Soetaert and Herman (1995). The Scheldt estuary is a heterotrophic, low-oxygen, nutrient-rich system with riverine dissolved inorganic nitrogen concentrations of >400 μmol L^{-1} (Struyf et al. 2004; Soetaert et al. 2005). Except for the period ranging from July to August, dissolved ammonium concentrations at Tielrode are generally high (>60 μmol L^{-1}), and concentrations decrease toward the more seaward part of the estuary. Consequently, nitrification has been identified as an important process in the water column of this estuary, accounting not only for the oxidation of ammonium but also for a significant fraction of the carbon fixation and oxygen demand (Soetaert and Herman 1995).

The study area is located in the northern end of the ~100,000 m^2 Tielrode Marsh (Fig. 1a). This triangular 3,477 m^2 section of the marsh is isolated on two sides by dikes, and water is fed into the area by only one high-order tidal creek (Fig. 1b). Groundwater input is negligible, as the marsh is higher than the neighboring embanked polder. Prior to arriving at the study area, the tidal water has traveled a considerable distance (~1 km) from the main river through tidal marsh creeks. During the entire experimental period, the southern boundary of the study area was screened off by 1-m–high wooden screens embedded 10–20 cm into the sediment (Fig. 1b). Only the 4.5-m–wide span of the tidal creek and creek banks were not screened off. Instead, a flume channel was constructed by placing 3-m–long boards along the creek. Tidal water could thus only enter and exit the study area via the creek, and surface water covering the study area during high tide was partitioned from that overflowing the remaining marsh. A 4.5-m–long sampling and tracer release platform was placed across the creek at the entrance to the study area.

The vegetation in the study marsh is typical for freshwater marshes, with large patches of common reed (monospecific stands of *Phragmites australis)* in the lower elevations, and willows (2–6-m–high specimens of *Salix* sp.) and ruderal vegetation (dominated by *Impatiens grandulifera, Epilobium hirsutum* and *Urtica dioica*) at the higher elevations (Fig. 1b). The vegetation cover is very dense, with *P. australis* and *I. grandulifera* growing to exceptional heights of up to 4 m, as is commonly observed in Scheldt marshes. Three sampling stations within each of the vegetation types and on unvegetated creek banks were made accessible by walking boards. Marsh sampling stations within each vegetation type were chosen to represent the variation in topography as well as distance from the sampling bridge. Benthic microalgal mats dominated by the filamentous yellow–green alga *Vaucheria* sp. were abundant throughout the marsh, particularly in the creek bank and willow sites. A digital terrain model of the study area was constructed using a geographic information system and a detailed mapping of the topography.

The entire study area is flooded only at the highest tides (26% of the tides), and the experiment was initiated just before a spring tide on 24 May 2002, when a maximum of consecutive high tides followed (12 tides), and sampling

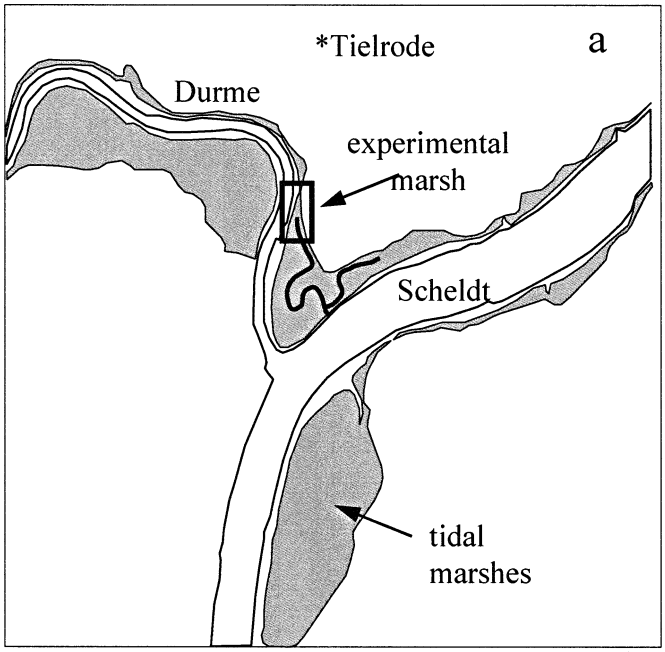

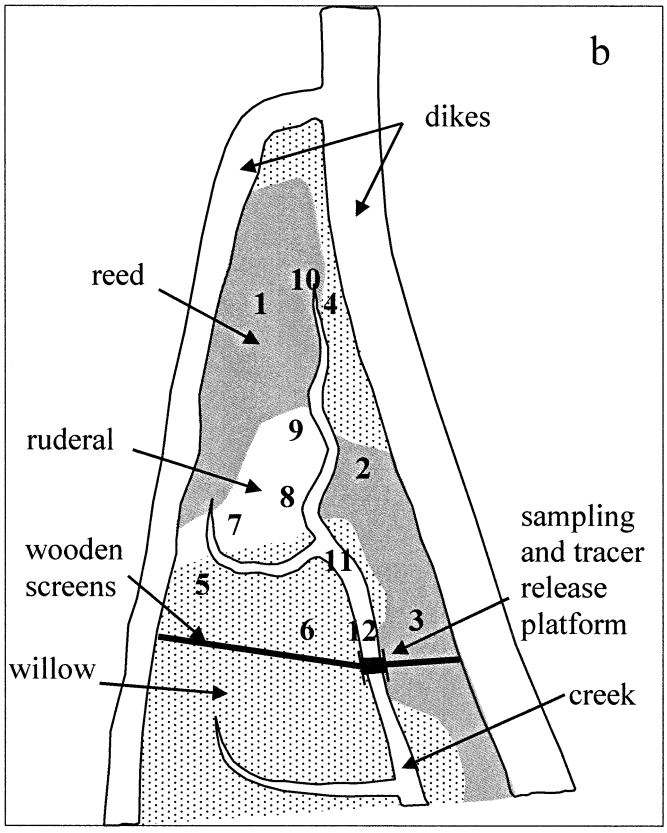

Fig. 1. (a) Tielrode tidal freshwater marsh fringing the Scheldt and Durme Rivers, with location of experimental marsh marked and (b) experimental marsh with vegetation distribution. Numbers represent sampling stations.

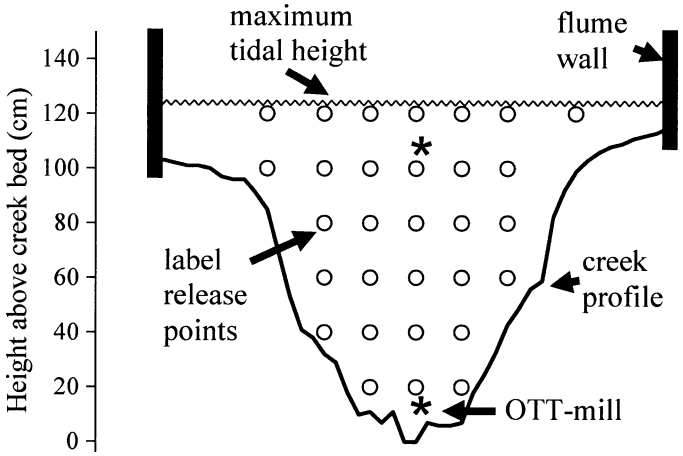

Fig. 2. Cross section of creek below sampling platform indicating labeling release points (o) and OTT-mill flow meters (*). Span between flume walls was 4.5 m. Label was released on the landward side of the 1.5-m–wide labeling platform, while flow measurements were conducted on the river (downstream) side.

continued until the following spring tide cycle 31 tides after labeling (10 June 2002), when the entire study area was once again flooded. Measurements were carried out prior to labeling (T_{-2}) to establish natural abundance levels of ^{15}N; at the tide when tracer was released (T_0), and at five subsequent tides (T_1, T_2, T_5, T_9, and T_{31}). The subscript denotes the tide number relative to tracer release.

Tracer release—On 25 May 2002 (T_0), 1.98 moles of ^{15}N-ammonium was added to the floodwater entering the study area. The tracer solution consisted of 1,247 g of 10.7% ^{15}N labeled ammonium sulfate [$(NH_4)_2SO_4$] and 50 kg of the conservative tracer NaBr dissolved in 250 liters of deionized H_2O. The added tracer increased the ^{15}N content of the ammonium pool to 1.3% and increased the total NH_4^+ concentration by approximately 14% (but *see* following). An even distribution of ^{15}N tracer throughout the marsh was accomplished by adding the tracer solution to the incoming tidal creek water proportionally to the water volume entering the study area. For this purpose, a simple tracer addition device was constructed. A 4.5-m–long, 24-mm–diameter polyvinyl chloride (PVC) pipe was placed on the railing of the sampling platform 2.67 m above the creek bed, fitted with 30 outlets and 150-cm–long 3.2-mm (inner diameter [ID]) Tygon tubing attached to each outlet. Each of the 30 outlet tubes was fitted with a clamp and placed into open PVC pipes (15-mm ID) attached vertically to the bridge and ending at various heights above the creek bed (release points, Fig. 2). Thus, three, four, five, five, six, and seven open pipes ended 20, 40, 60, 80, 100, and 120 cm above the creek bed, respectively. During floodwater labeling (T_0), tracer flowed passively from an elevated small reservoir (25 liter) into the main pipe, where pressure, and thus the tracer flow rate through open valves, were kept constant (2.5 mL s^{-1}) by maintaining a constant solution level in the small reservoir. The tracer level in the small reservoir was kept constant by continuously pumping tracer solution from a larger tank into the small reservoir, where a closed overflow returned excess

tracer solution to the large tank. Tests prior to deployment confirmed that the flow out of each individual outlet was the same regardless of how many outlets were open. Enrichment solution then dripped via the Tygon tubes into the vertical pipes. The number of outlets open was continuously regulated to maintain a constant degree of labeling. Thus, initially, only outlets to the lowest situated release points were open, but as the water level and flow velocity in the creek rose, an increasing number of outlets releasing tracer higher above the creek bed were manually opened. Labeling was initiated when the first floodwater arrived at the sampling and tracer release platform.

Creek-water sampling and analysis—Creek water was sampled from the sampling bridge using an 80-cm–long (6-cm ID) water sampler fitted with a bottom valve. Care was taken to get an integrated water sample over the entire water column. At each time point, three samples were pooled and a 1-liter subsample was immediately brought to the field laboratory. Twelve creek-water samples were collected during the main tide, defined here as the duration from floodwater arrival below sampling platform until there was no change in water level for 30 min (flood + ebb), and three were collected from the seepage water during low tide. Additional 1-liter floodwater samples were collected from the 12 marsh sampling stations at high water during T_0 (maximum tide) and from the main river (the Scheldt).

Water samples (300–500 mL) were immediately filtered under vacuum through precombusted, preweighed GF/F Whatman filters. The filters were stored frozen for particulate ^{15}N nitrogen analysis (*see* following). Filtered water samples (30 mL) for isotopic composition analysis of ammonium and nitrate were immediately transferred to 100-mL Schott bottles, capped tightly, and stored frozen. Replicate samples for determination of $^{15}N_2O$ and $^{15}N_2$ were preserved with 500 or 50 μL NaOH (2 mol L^{-1}) in tightly capped (gas-tight crimp-seal septum) 60-mL and 20-mL headspace vials, respectively, stored at room temperature with no headspace, and were analyzed within 1 week. Preserving the samples with NaOH also trapped the carbon dioxide from the headspace later introduced for analysis (*see* following). Filtered subsamples for determination of NH_4^+, NO_3^-, and NO_2^- concentration were stored cold (4°C) and analyzed within 3 d, while samples for Br^-determination were stored frozen.

Nitrogen isotopic compositions of NH_4^+ and $NO_3^- + NO_2^-$ were determined in two steps using a modification of the ammonia diffusion procedure (Sigman et al. 1997; Holmes et al. 1998), followed by mass spectrometry. Briefly, 30-mL filtered water was transferred to a 100-mL Scott incubation bottle and 0.1 g NaCl was added. $^{15}NH_4$ was determined by adding MgO, converting NH_4^+ to NH_3, which was trapped on an acidified (H_2SO_4) 10-mm GF/D filter sandwiched between two Teflon filters floating on the sample surface. After 8 d of shaking at room temperature, filters were removed, dried for 2 d in an exicator, and analyzed using a Fisons elemental analyzer (EA-1500) coupled online via a Finnigan CONFLO II interface, with a Finnigan Delta S isotope ratio mass spectrometer (EA-IRMS). Tests confirmed complete ammonium removal from samples after 8 d of incubation. Devarda's Alloy was subsequently added to the sample to convert $NO_3^- + NO_2^-$ to NH_3, which was collected onto a new acidified filter as described above. Bulk suspended particulate nitrogen (SPN) on GF/F filters was determined after drying (6 h, 60°C) using a Carlo–Erba CN analyzer following Nieuwenhuize et al. (1994) and the isotopic composition determined by EA-IRMS (described previously).

Dissolved nitrous oxide (N_2O) concentrations and isotopic composition in headspace gas (10 mL He headspace in 60-mL vials, then shaken for 30 min) were determined by gas chromatography coupled to isotope ratio mass spectrometry (GC-IRMS, Hewlett Packard G1530 GC, with Thermo Finnigan Delta-plus IRMS). The GC was fitted with a Poraboud Q column (dimensions: length, 50 m; 0.32-mm ID; film, 5 μm, Chrompack) operated at 30°C with a 2 mL min^{-1} column flow of helium. The oxidation and reduction reactors of the GC-IRMS interface were bypassed. A sample of the headspace (500 μL) was injected in split mode (split ratio: 1 : 10) at 110°C. Concentrations were calibrated against a certified gas mixture (5 ppmv N_2O) and recalculated to water concentrations using the temperature- and salinity-dependent partitioning coefficient (Weiss and Price 1980). Stable isotope ratios of N_2O were measured on masses 44 and 45 and calibrated against carbon dioxide reference gas. Reported ^{15}N : ^{14}N-ratios are based on the average of multiple gas injections from the same sample. This method of N_2O analysis is very sensitive for N_2O concentrations, and good results were obtained for the complete tidal cycle. Although our method of stable isotope analysis is not optimal for natural abundance ^{15}N studies, precision was sufficient (standard deviation [SD] above 40 nmol L^{-1} N_2O, approximately 0.020 atom% ^{15}N) to detect significant labeling of the N_2O pool during the main tide (*see Results*). Isotopic composition of dissolved dinitrogen ($^{29}N_2$, $^{30}N_2$) in headspace gas (2 mL He headspace in 20-mL vials) was determined by EA-IRMS equipped with a Haysep Q column. Samples were injected directly in front of the EA chromatography column. Results are based on the average of three gas injections from the same sample. For calculations of enrichment of the total N_2 pool, an equilibrium concentration of 550 μmol L^{-1} (20°C) was assumed.

Nutrient concentrations were measured colorimetrically on an automated Segmented Flow Analyzer. Bromide concentrations were determined by high-pressure ion chromatography with ultraviolet detection.

Ex situ rate measurements—Water-column nitrification rates (WNR) (T_{-2}, six times over the tidal cycle) were determined in bottle incubations by measuring the transfer of ^{15}N in ammonium to nitrate according to a modification of Horrigan et al. (1990). Briefly, creek-water samples were spiked with $^{15}NH_4Cl$ (98 atom%) to approximately 2% of the ambient NH_4^+ concentration and incubated in the dark at in situ temperature in 100-mL Scott bottles for 3 h. Incubations were ended by filtration through precombusted Whatman GF/F filters (21 mm), the ^{15}N content of NH_4^+ and $NO_3^- + NO_2^-$ in the filtrate measured by the diffusion method described above and nitrification rate calculated from the (linear) increase of ^{15}N in $NO_3^- + NO_2^-$. Absolute uptake rate of ammonium (μmol N L^{-1} h^{-1}) into the particulate nitrogen

Table 1. Duration of main tide (flood and ebb), maximum water height above creek bed (2.47 m above mean sea level) below measuring platform, water volume estimated from the digital terrain model, and calculated water budget computed by mass balance model during the seven tides. Values in parentheses are balances in percentage of flood.

	Duration		Water	Water	Water budget				Import in %	Export in %
Tide	Flood (min)	Ebb (min)	height (cm)	volume* (m^3)	Flood (m^3)	Ebb (m^3)	Seepage (m^3)	Balance (m^3)	of total volume† (%)	of total volume‡ (%)
T_{-2}	78	107	105	1,336	1,234	1,206	66	−38 (−3.1)	92	95
T_0	80	131	125	2,099	1,823	2,103	65	−345 (−18.9)	87	103
T_1	77	119	117	1,800	1,700	1,642	61	−3 (−0.2)	94	95
T_2	82	144	136	2,511	2,364	2,580	64	−277 (−11.7)	94	105
T_5	78	139	129	2,249	1,912	2,218	65	−372 (−19.5)	85	102
T_9	79	120	109	1,500	1,376	1,305	65	7 (0.5)	92	91
T_{31}	76	106	100	1,173	900	955	68	−123 (−13.7)	77	87

* Calculated from the digital terrain model and maximum water height.
† Calculated floodwater volume from mass balance model in percentage of water volume estimated from *.
‡ Calculated ebb water volume + seepage from mass balance model in percentage of water volume estimated from *.

pool (PN) was determined according to Middelburg and Nieuwenhuize (2000).

Discharge characteristics and additional measurements—Two OTT-mill flow meters continuously (at 1-min intervals) measured current velocity at the bottom and surface of the creek center. The bottom flow meter was fixed ~20 cm above the creek bed, the top one maintained at ~30 cm below the water surface, according to the tidal level (monitored every minute). In addition, lateral surface flow rates were measured every 5–10 min at fixed points (0.5-m interval) between the flume walls with an electromagnetic flow meter (EMF, Valeport Model 801). During the seepage phase, here defined as the period after the main tide during which no decrease in water level was observed for 30 min, EMF measurements were conducted every hour. The creek profile was subdivided into lateral subsegments and discharge calculated per minute in each segment by multiplying the cross-sectional area of the channel by water velocity. These data were used to calculate advective water fluxes in and out of the study area.

Dissolved oxygen, specific conductivity, temperature, pH, and turbidity were recorded continuously (at 2-min intervals) during all tides using a Hydrolab Datasonde 3.

Water traps in the marsh—To evaluate if the $^{15}NH_4^+$ tracer successfully mixed with the floodwater and was distributed evenly over the entire study area, water traps were placed at each marsh sampling station (Fig. 1b) during T_0. Each water trap consisted of eight 30-cm–long PVC pipes (15-mm ID) attached at 10-cm height intervals to a bamboo pole. As the water rose over the marsh surface, pipes captured water at 10-cm depth intervals, with the lowest trap collecting initial floodwater and highest trap capturing water at high tide. Rhodamine addition tests revealed negligible mixing with overlying water once traps were filled. Traps were sampled with a 30-mL syringe by withdrawing 10 mL via a polyethylene tube gently inserted to the bottom of the trap. Water traps were sampled immediately following T_0 and analyzed for Br^- (conservative tracer) as described previously.

Calculations—Water budgets for each tide were calculated from the measured water flows (Table 1). Furthermore, the total volume of water covering the study area in a given tide and duration of water cover at each sampling station were calculated from the digital terrain model using the maximum water levels measured at the sampling platform. Stock size for all components dissolved or suspended in the water column over the tidal cycle were calculated from concentration and discharge measurements for each sampling point.

Nitrogen isotopic ratios are expressed in the delta notation ($\delta^{15}N$, ‰) relative to atmospheric nitrogen and mostly given as $\Delta\delta^{15}N$ (isotopic enrichment), corrected for natural abundance levels of ^{15}N by subtracting the $\delta^{15}N$ value of similar samples collected at the same time relative to maximum tide at $T_{(-2)}$. The tracer content (excess ^{15}N) in each nitrogen pool was determined from the isotopic enrichment and stock size, and a total ^{15}N inventory and ^{15}N-flow balance was constructed for each tide. Similar inventories were made for the conservative tracer (Br^-) and unlabeled nitrogen pools. Net ecosystem nitrification rate was calculated from the net transfer of ^{15}N from the added ammonium tracer pool to the nitrate pool over the first tide (T_0) (^{15}N mass balance) and from the linear increase in isotopic enrichment of $NO_3^- + NO_2^-$ during T_0 ebb.

Air–water exchange fluxes of $^{15}N_2O$ and $^{15}N_2$ were calculated from the product of gas transfer or piston velocity (k) and the partial pressure of the gas. Gas transfer velocities in estuaries depend on various factors, including current velocity, wind velocity, and fetch, and we have therefore calculated a lower and upper limit based on k values of 5 (in the absence of wind) and 50 cm h^{-1}, the range of observations in the Scheldt estuary (Borges et al. 2004). Water surface area available for exchange was based on water height and digital terrain model.

Results

Hydrodynamics and creek characterization—The average tidal cycle in the creek showed a normal diurnal sinusoidal tide. The flood lasted ~80 min (Table 1), and after high tide,

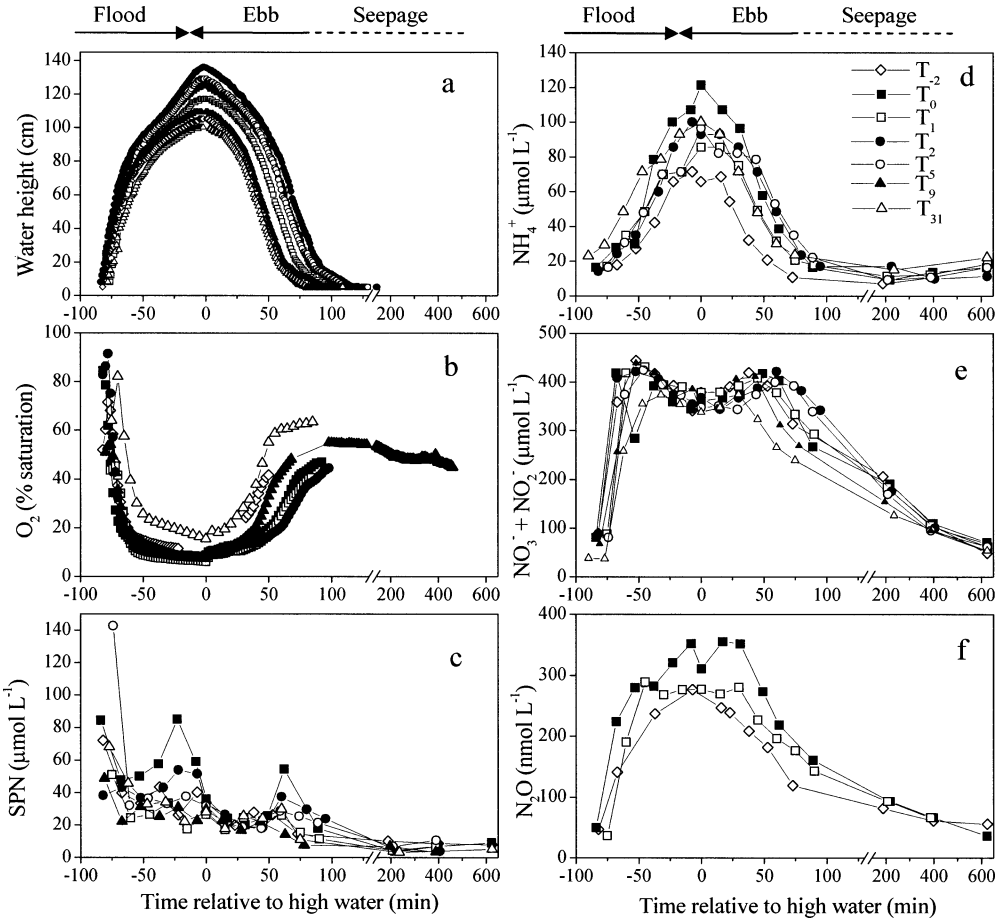

Fig. 3. Water level, O_2, and nitrogen pools in the creek below the sampling platform as a function of time relative to maximum tidal height in all seven tides. (a) Water height, (b) O_2 saturation, (c) suspended particulate nitrogen concentration (SPN), (d) dissolved ammonium concentration (NH_4^+), (e) dissolved nitrate and nitrite concentration ($NO_3^- + NO_2^-$), and (f) dissolved nitrous oxide concentration (N_2O). The three phases of the tidal cycle (flood, ebb, and seepage) are indicated above figures, with arrow indicating the direction of the water flow.

the water dropped according to a normal tidal curve until the bottom of the creek was nearly reached (Fig. 3a). The main ebb lasted for 106 to 144 min depending of the tidal height. Then water seeping out of the sediment and between vegetation kept flowing out (average speed ~6 cm s^{-1}) until the next flood (after 8.5–9.5 h). Current speeds in the creek strongly depended on the level of the high tide, but the same spatial pattern was observed during all seven tides. Flood currents were relatively constant (~20 cm s^{-1}), while ebb currents showed more variation (20–50 cm s^{-1}) with time and depth. Maximum ebb current were up to 66% faster than maximum flood current and current speeds were always higher near the surface than at the bottom (up to 60% higher). The amount of water covering the study area estimated by the digital terrain model varied by a factor of 2.1 among the seven tides studied, while the calculated amount of water entering and leaving the marsh varied by factors of 2.6 and 2.5, respectively (Table 1). Except for T_9, the exported water volume exceeded the incoming volume. The calculated export generally deviated less from the volume estimated by the digital terrain model than the estimated import volume, indicating the import to be underestimated. However, Br^- mass balance during T_0 indicates the ebb water budget to be slightly overestimated (*see* following). Between tides, 65 ± 2 m^3 water (seepage) was exported, corresponding to 2.5–7.1% of the total water volume depending on maximum tidal height.

Water temperature and pH varied from 17°C to 19°C and from 7.4 to 7.7 across all tides, respectively. Except at T_0 maximum tide, when the conservative tracer (Br^-) increased the conductivity by 30% (*see* following), conductivity was relatively constant (~1 mS cm^{-1}) over the tidal cycle and between tides. Initial turbidity in the floodwater was high (80–200 nephelometric turbidity units [NTU]), but turbidity decreased rapidly to <50 NTU in most tides. In the highest tides, however, turbidity remained high during flood and the first part of the ebb, showing erratic temporal patterns. The initial floodwater was relatively oxic (40–90%), but dissolved oxygen concentrations rapidly decreased to ~10% saturation, and the water was hypoxic (<50 μmol L^{-1}) during most of the main tide (Fig. 3b). During ebb [O_2] increased linearly ($r^2 = 0.92$, $p < 0.01$) as a function of de-

Table 2. Vegetation type, topographic level (relative to mean sea level), duration of flooding at T_0, and water trap bromide concentrations (T_0) at the 12 sampling stations. Water traps are divided into traps placed above and below 3.4 m above mean sea level. Locations of sampling stations are shown in Fig. 1b.

Vegetation type	Station no.	Surface height (m)	Flooding duration (T_0) (min)	Bromide	
				<3.4 m (μmol L^{-1})	>3.4 m (μmol L^{-1})
Reed	1	3.23	117	339±54	189±23
	2	2.97	139	352±80	239±53
	3	3.06	133	323±11	250±12
Willow	4	3.15	124	381±63	331±32
	5	3.34	105	—	228±26
	6	3.40	92	—	292
Ruderal	7	3.31	109	—	230±22
	8	3.25	116	358	262±31
	9	3.31	109	262	235±6
Creek	10	3.11	129	366	283±23
	11	2.87	148	360±16	371±5
	12	2.67	163	385±50	264±51

creasing water height to ~50% saturation at the end of all tides. Generally, T_{31} water was slightly higher in dissolved oxygen compared to the other tides.

Ammonium concentrations in the floodwater varied greatly and revealed a bell-shaped distribution pattern over the tidal cycle (Fig. 3d). Initially below 20 μmol L^{-1}, concentrations gradually increased to 60–120 μmol L^{-1} at maximum tide, followed by a gradual decrease to 10–20 μmol L^{-1} at the end of the main ebb tide. During seepage, a slight increase in $[NH_4^+]$ was observed. Similar patterns were observed in all tides, but the maximum concentration varied by a factor of two between tides. Only at maximum tidal height did $[NH_4^+]$ match that of the main river (105–120 μmol L^{-1}). $[NH_4^+]$ was inversely correlated with O_2 saturation ($O_{2\%}$) ($[NH_4^+] = 463.5 \times O_{2\%}^{-0.83}$; $r^2 = 0.79$, $p < 0.001$). The $NO_3^- + NO_2^-$ concentrations showed a bimodal distribution curve over the tidal cycle (Fig. 3e). From relatively low (40–90 μmol L^{-1}) concentrations in the initial floodwater, $[NO_3^-] + [NO_2^-]$ rapidly increased to 400–450 μmol L^{-1} halfway into the flood period, but subsequently decreased slightly to ~350–400 μmol L^{-1} at maximum tide. Following a second $[NO_3^-] + [NO_2^-]$ peak midway through the ebb tide, concentrations gradually decreased to ~250–350 μmol L^{-1} at the end of the main tide and continued to decrease in the seepage. During most of the main tide, $[NO_3^-] + [NO_2^-]$ was significantly higher than in the main river (300–320 μmol L^{-1}). Nitrite (NO_2^-) accounted for 2–17% of the $NO_3^- + NO_2^-$, with maximum contributions at maximum tide. Overall, the dissolved inorganic N pool (DIN $= NH_4^+ + NO_3^- + NO_2^-$) was relatively constant (450–480 μmol L^{-1}) for the main duration of all tides. From the end of ebb, however, [DIN] gradually decreased to relatively low (60–100 μmol L^{-1}) concentrations in the seepage water. Similar low concentrations were observed in all initial floodwater samples. Onward $NO_3^- + NO_2^-$ will collectively be referred to as nitrate (NO_3^-).

Nitrous oxide (N_2O) concentrations were only determined in the first three tides, in which the temporal patterns roughly mimicked that of nitrate, but concentrations were three orders of magnitude lower (Fig. 3f). Concentrations of SPN were generally highest (40–148 μmol L^{-1}) in the initial floodwater, but decreased with time (Fig. 3c). In the three highest tides (T_0, T_2, and T_5), additional peaks in SPN coincided with maxima in flow rates and turbidity during flood as well as ebb. Low [SPN] (3–11 μmol L^{-1}) was always observed in the seepage, likely reflecting particle settling, consistent with low NTU values.

Conservative tracer distribution—Addition of a conservative tracer (NaBr) to the tracer solution enabled us to monitor the distribution of the label within the study site and indeed verified that a rather even distribution was obtained (Table 2). Bromide concentrations were, however, slightly higher (0.35 ± 0.05 mmol L^{-1}) in lower-placed water traps than in higher ones (0.27 ± 0.06 mmol L^{-1}), indicating that tracer was initially released at a slightly higher relative rate than during the bulk of the tide. The peak in bromide concentration (0.6 mmol L^{-1}) in the first sample of the outgoing tide shows that tracer addition was carried out for too long and/or at too high a rate at the turn of the tide (Fig. 4). It appears that the tracer addition valves were not closed sufficiently fast at the rather abrupt halt in tidal inflow. However, this last labeled body of water quickly left the creek again and therefore did not mix with the main body of water covering the marsh. The very uniform concentration (0.26 ± 0.02 mmol L^{-1}) in the remaining water leaving at T_0 together with the water trap (Table 2) and T_0-maximum tide water samples (0.24 ± 0.11 mmol L^{-1}) substantiate that the tracer was relatively evenly distributed over the entire study area. Recovery of the added Br^- in the mass balance (T_0) was 115%, indicating that the ebb water volume during T_0 was overestimated. In addition, bromide was slightly elevated in the last part of the outflow of $T_1 - T_5$, with minor influence on the Br^- mass balance due to low water volumes.

Stable isotopes—The ammonium pool in the T_0 ebb water (directly after the ~80-min period of tracer addition to the floodwater) was enriched 1,975–4,735‰ ($\Delta\delta^{15}NH_4^+$) (Fig. 5a). Enrichment of samples collected from the 12 marsh sampling stations at T_0-maximum tide was well within this

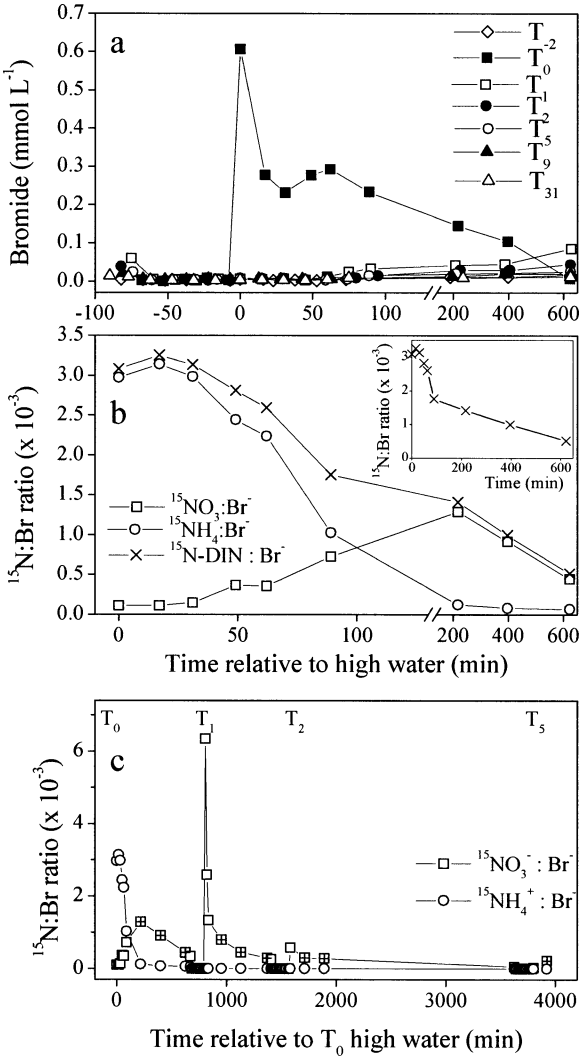

Fig. 4. (a) Bromide concentration in the floodwater during the seven tides in relation to time relative to maximum tidal height; (b) changes in ratio between excess ^{15}N in NH_4^+, NO_3^-, and DIN and conservative tracer Br^- concentrations during T_0 ebb and seepage (insert shows DI^{15}N : Br^- on an unbroken time scale); and (c) changes in ratio between excess ^{15}N in NH_4^+, NO_3^-, and DIN and conservative tracer Br^- concentrations from end of label addition (T_0-maximum) to T_5. Symbols with (+) indicate seepage phase. Note the different scales on the x-axis.

range (2,878 ± 844‰). The initial peak in ebb water $\Delta\delta^{15}NH_4^+$ is attributed to overlabeling around the turn of the tide (*see Conservative tracer distribution*). In the seepage water, the enrichment decreased over time from 545‰ to 119‰, indicating dilution with unlabeled NH_4^+ from mineralization or exchange with particulate pools. In following tides, only the initial flood sample of T_1 showed significant enrichment (69‰) of the ammonium pool (Fig. 5a, insert).

^{15}N enrichment to the nitrate pool was observed immediately around the turn of the T_0 tide, and enrichment increased linearly over time to 175‰ at the end of the main tide (Fig. 5b). Enrichment was even higher (269‰) in the first seepage sample (217 min after T_0-maximum), but subsequently decreased to 170‰ over the following 7 h. In the following two tides (T_1 and T_2), the initial floodwater was enriched in ^{15}N-nitrate (91‰ and 31‰, respectively), then decreased to below <10‰ enrichment, followed by a gradual increase in the ebb and seepage water (to 54‰ and 23‰, respectively). The temporal ^{15}N enrichment pattern of SPN was similar to that of the nitrate pool, except the maximum enrichment was much lower (75‰) and occurred at the end of the ebb tide and not during seepage (Fig. 5c). The enrichment was predominantly in the smallest, most abundant SPM fractions (<20 μm) (data not shown).

Coinciding with the ^{15}N enrichment to the nitrate pool, the nitrous oxide pool was also enriched during T_0 and T_1 (Fig. 5d). The enrichment increased linearly (T_0) and was ~50% higher (up to 399‰) than in the nitrate pool. The isotopic composition of N_2O could only be determined during the main tide and in the initial seepage sample. A slight but significant increase (2‰) in ^{15}N was observed in the N_2 pool during T_0 seepage (Fig. 5e), indicating the occurrence of denitrification.

The initial excess concentration of ^{15}N-NH_4^+ (calculated as the measured ^{15}N-NH_4^+ concentration minus the natural abundance concentration) in the T_0 ebb water was high (1.8 μmol L^{-1}; Fig. 5f), since too much label was added at the end of the label addition period (*see Conservative tracer distribution*). Thereafter, the concentration of excess ^{15}N-NH_4^+ was relatively constant (0.7 μmol L^{-1}) for the main duration of the ebb tide but decreased to 0.3 μmol L^{-1} toward the end of the main tide. Removal of ^{15}N from the ammonium pool during T_0 was, however, clearly evident from the decrease in $^{15}NH_4^+ : Br^-$ concentration ratio from 3.1×10^{-3} initially to 1.0×10^{-3} at the end of the ebb tide (Fig. 4b). In the seepage water following T_0 and initial T_1 samples, low concentrations of ^{15}N-NH_4^+ were detected. Thereafter, $^{15}NH_4^+$ concentrations were not significantly different from natural abundance levels.

The temporal pattern of excess $^{15}NO_3^-$ (Fig. 5g) roughly mimicked that of the $\Delta\delta^{15}NO_3^-$, except that the maximum at T_0 was observed in the seepage and at the end of ebb in the following tides. During T_0 ebb, the concentration of excess $^{15}NH_4^+$ decreased 4.15 times faster than the corresponding excess $^{15}NO_3^-$ concentration increased (inferred from slopes of curves in Fig. 5f,g), indicating that 24% of the transformed ^{15}N ammonium was nitrified. An increase in the $^{15}NO_3^- : Br^-$ concentration ratio over time further demonstrates incorporation of ^{15}N into the nitrate (NO_3^-) pool during T_0 (Fig. 4b). In subsequent tides, high $^{15}NO_3^- : Br^-$ concentration ratios were also observed, especially halfway through T_1 ebb, at which time $^{15}NO_3^- : Br^-$ was twice as high as $^{15}N : Br^-$ in the tracer solution (Fig. 4c). Overall, the excess dissolved inorganic ^{15}N (DI^{15}N) : Br^- concentration ratio decreased linearly during both T_0 ebb and seepage, but the decrease was one order of magnitude faster during ebb (Fig. 4b, insert). This decreasing ratio further demonstrates that NO_3^- was not the only sink for $^{15}NH_4^+$. Excess ^{15}N concentration in the particulate pool showed a temporal pattern similar to nitrate (Fig. 5h), but concentrations were more than one order of magnitude lower.

Excess ^{15}N-N_2O concentrations (Fig. 5i) mimicked those of nitrate over the tidal cycle, but concentrations were three orders of magnitude lower. Estimated water–air gas ex-

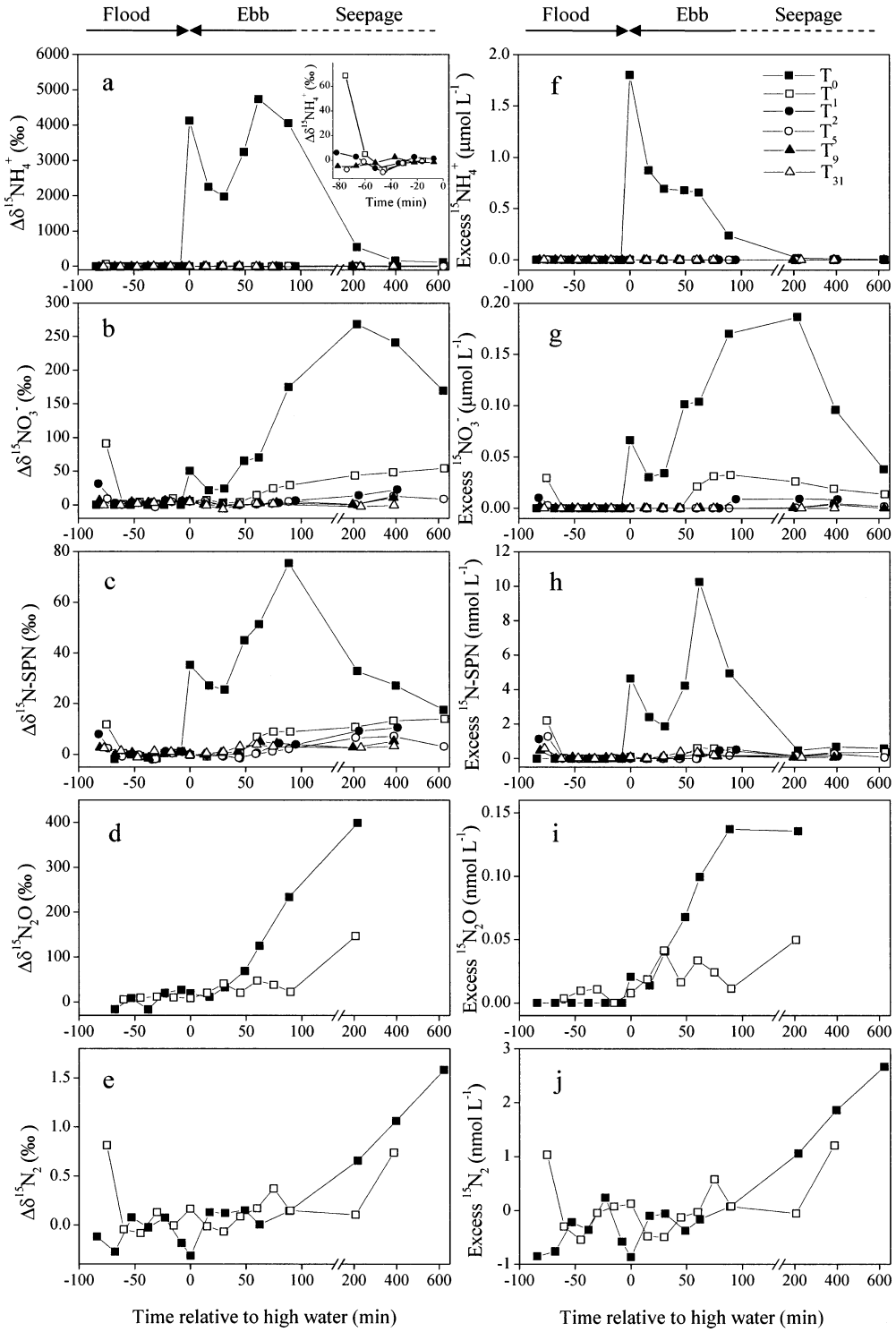

Fig. 5. Isotopic enrichment ($\Delta\delta$) (above natural abundance level) in (a) NH_4^+, (b) NO_3^-, (c) SPN, (d) N_2O, and (e) N_2, and excess ^{15}N concentration of (f) $^{15}NH_4^+$, (g) $^{15}NO_3^-$, (h) ^{15}N-SPN, (i) N_2O, and (j) N_2 in the floodwater of the six tides. Insert in panel a shows an enlargement of the lower left part of panel a. The three phases of the tidal cycle (flood, ebb, and seepage) are indicated above figures, with arrow indicating the direction of the water flow.

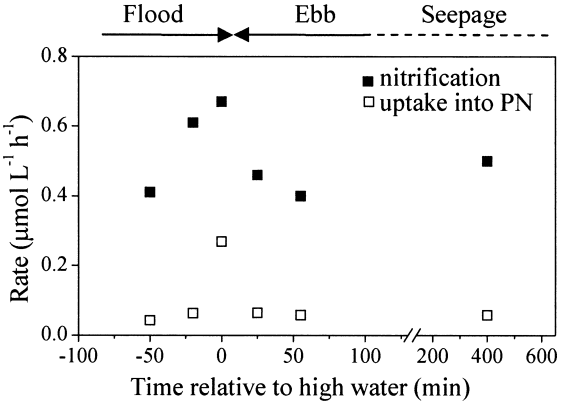

Fig. 6. Nitrification rate and rate of ammonium uptake into the suspended particulate nitrogen (PN) pool in closed-bottle water incubations. The three phases of the tidal cycle (flood, ebb, and seepage) are indicated above figures, with arrow indicating the direction of the water flow.

change from the entire water surface could account for a loss of 6–60 μmol ^{15}N-N_2O to the atmosphere during the main T_0 tide. During T_0 seepage, the concentration of excess $^{15}N_2$ increased linearly to 2.7 nmol L^{-1} (Fig. 5j). No ^{15}N was recovered in the N_2 pool during the main tide, and estimated water–air exchange of $^{15}N_2$ was zero. Sediment–air gas exchange during emersion was not determined.

Nitrogen transformation rates—Bottle incubations with ^{15}N revealed WNR rates of 0.40–0.67 μmol L^{-1} h^{-1} over the T_{-2} tidal cycle (Fig. 6). WNR were linearly correlated with $[NH_4^+]$ ($r^2 = 0.80$, $p < 0.05$), except during seepage, when relatively high rates were observed. WNR were seven to ten times higher than uptake rates of ammonium into the particulate pool, except in one ebb sample, in which exceptionally high (0.27 μmol L^{-1} h^{-1}) uptake rates were observed.

In situ transfer of ^{15}N from the added ammonium to the nitrate pool as a result of nitrification is directly evident from the increase in $\Delta\delta^{15}NO_3^-$ during T_0 ebb (Fig. 5b). A simple estimate of whole-ecosystem nitrification rate during marsh flooding can be obtained from the linear increase ($r^2 = 0.93$, $p < 0.05$) in the excess ^{15}N-NO_3^- concentration (Fig. 5g) during T_0 ebb tide. Assuming complete symmetry of the flow patterns of flood and ebb and no or limited mixing of the water (i.e., the first body of water entering the study area is the last to leave), the net ecosystem nitrification rate (ENR) can be expressed according to:

$$\mathrm{ENR}_{\mathrm{regression}} = \frac{\alpha}{\%^{15}\mathrm{N}_{\mathrm{NH_4}}} \quad (1)$$

where α is the slope of excess $^{15}NO_3^-$ during T_0 ebb as a function of 2× sampling time after T_0-maximum (accounting for residence time effectively being twice the duration between T_0-maximum and sampling time), and $\%^{15}N_{NH_4}$ is the average percentage of the ammonium pool labeled with ^{15}N. Another estimate of ENR during T_0 can be determined from mass balance calculations according to:

$$\mathrm{ENR}_{\mathrm{mass\text{-}balance}} = \frac{\Sigma^{15}\mathrm{NO}_3^-}{V \times T \times \%^{15}\mathrm{N}_{\mathrm{NH_4}}} \quad (2)$$

Table 3. Nitrification rate estimates for the water phase (WNR) and whole marsh ecosystem (ENR). Water phase incubations were done during T_{-2}, while whole ecosystem rates were determined from T_0.

Compartment	Method	Nitrification rate (μmol L^{-1} h^{-1})
Water phase	^{15}N bottle incubations	0.5±0.1
Whole ecosystem	Regression (Eq. 1)	4.6
	^{15}N mass balance (Eq. 2)	2.0
	Nutrient mass balance*	−7.3–21.2

* All seven tides, derived from NO_3^- mass balance.

where $\Sigma^{15}NO_3^-$ is the total amount of $^{15}NO_3^-$ exported during T_0 ebb, V is the total water volume in the study area, T is the duration of the main tide (flood + ebb), and $\%^{15}N_{NH_4}$ is the average percentage of the ammonium pool labeled with ^{15}N. Both estimates of ENR are significantly (four to nine times) higher than WNR (Table 3), revealing that the marsh system as a whole is an intense site for nitrification and that most nitrification was associated with sediment and biofilms rather than the water column. Similarly, a mass-balance estimate of the uptake rate of $^{15}NH_4^+$ into SPN is almost twice as high (0.11 μmol h^{-1}) as those measured in most bottle incubations (0.06 ± 0.1; exceptionally high value at maximum tide excluded; Fig. 6).

The N_2O production rate based on the linear increase in $^{15}N_2O$ concentration (Fig. 5i) and calculated using the same approach as $\mathrm{ENR}_{\mathrm{regression}}$ was 6.96 nmol L^{-1} h^{-1}, while a rate of 1.41 nmol L^{-1} h^{-1} was obtained from the $^{15}N_2O$ mass balance. The NO_3^- to N_2O ratio was 663 to 1,441, based on the regression and mass-balance approaches, respectively. Including seepage water in the mass-balance estimates rendered a similar $NO_3^-:N_2O$ ratio (1,446 : 1).

The fate of N—^{15}N mass-balance budgets revealed that 31% of the added tracer was either transformed or taken up by the marsh biota (Table 4). Of the 1.98 moles of ^{15}N added, 8.7% was nitrified, while 69% was exported as ammonium (unprocessed) during the first tide. An additional 0.5% was exported as SPN, and only 4% (T_0) was retained in the marsh (sinks = sediment, plants, roots, plant litter) (Gribsholt et al. unpubl. data). Collectively, less than 0.01% of the ^{15}N was recovered in dissolved gas (N_2O and N_2). The cumulative transfer of ^{15}N to the different pools changed only slightly in subsequent tides. Thus, the only difference was the amount of label recovered in marsh sinks other than nitrate that accounted for 6.9% and 5.0% after T_5 and T_{31}, respectively, while the importance of nitrification increased from 8.7% to 9.1% (Table 4). We were able to account for 83–86% of added ^{15}N. The remaining 14–17% was probably transferred to the dissolved organic nitrogen (DON) pool and exported during ebb water or was denitrified and lost to the atmosphere as N_2 during low tide (sediment–air flux) (*see Discussion*). Nitrification was quantitatively the most important transformation process for ^{15}N.

Whether the tidal freshwater marsh net imported or exported nitrate and/or ammonium could not be determined from the mass balance based solely on nutrient concentra-

Table 4. ^{15}N mass balance budget. Recovery in the various N-pools after T_0, T_5, and T_{31} (cumulative, except sinks). Numbers in parentheses are percentages of the total ^{15}N added.

Compartment	T_0 (mmol)	T_0–T_5 (mmol)	T_0–T_{31} (mmol)
Tracer input	1,976 (100)		
^{15}N exported unchanged (as $^{15}NH_4$)	1,370 (69)	1,369* (69)	1,369 (69)
^{15}N transformed	607 (31)		
$^{15}NO_3 + {}^{15}NO_2$	172 (8.7)	181 (9.1)	181 (9.1)
$^{15}N_2O$	0.13 (0.0)	0.13 (0.0)	0.13 (0.0)
$^{15}N_2$	0.11 (0.0)	0.11 (0.0)	0.11 (0.0)
$SP^{15}N$	9.6 (0.5)	10.0 (0.5)	10.0 (0.5)
SINKS†—stored	79 (4.0)	135 (6.9)	98.1 (5.0)
Balance not accounted for	345 (17)	280 (14)	318 (16)

* Decrease in export of $^{15}NH_4^+$ due to small amount pushed back into the marsh during T_1 flood.
† SINKS collectively refer to uptake into plants, roots, sediment, and plant litter.

tions. Although almost closed, proper error accumulation estimates showed that a balanced nitrogen budget based on concentration and water fluxes could not be derived. Thus, nitrate export relative to nitrate import varied between −4 and +26%, while ammonium export relative to import varied from −11 to +20% among the seven tides. Ammonium transformation rates (main tides) based on the mass balance varied between −1.8 and 3.2 μmol L^{-1} h^{-1}, while overall changes in nitrate ranged from −7.3 to 21.2 μmol L^{-1} h^{-1} (Table 3). Generally, the highest tides (including T_0) showed a net export of both NH_4^+ and NO_3^-, because ebb water estimates during these tides greatly exceeded flood (Table 1).

Discussion

Whole-ecosystem labeling—The relatively new technique of in situ stable isotope enrichment has increased our understanding of N processing under natural conditions. It allows for the examination of N flow through multiple pools simultaneously while maintaining natural hydrologic and biogeochemical gradients and ecosystem processes. Unconfined, whole-ecosystem ^{15}N enrichments have been carried out in lakes (Kling 1994), streams (Peterson et al. 1997; Hamilton et al. 2001; Wollheim et al. 2001), and estuaries (Holmes et al. 2000; Hughes et al. 2000; Tobias et al. 2003). The present study is, to our knowledge, the first of its kind in tidal marshes, and it yielded several new insights about the functioning of these ecosystems. First, our results unequivocally show that nitrification is one of the most important transformation processes associated with eutrophic freshwater marshes. Moreover, we demonstrated that the large reactive surface area of marsh sediment and biofilms is a key site for nitrification. Finally, we found that freshwater marshes function as nutrient transformers as well as nutrient sinks.

Numerous studies have attempted to draw inferences about marsh–estuarine interactions by measuring nutrient concentrations of flooding and draining water over tidal cycles (mass balance) (Merrill and Cornwell 2000). However, possible net changes are often obscured by large uncertainties in the hydrologic budget, which is also the case in this study. The mass-balance deficit in floodwater at most tides compared to mass-balance ebb water and estimates of maximum standing water volume (digital terrain model) indicate that some water enters the marsh through pathways other than the main creek. Though care was taken, screens transecting the downstream end of the marsh may not have been completely watertight, and water may have flown into the study area, where screens joined the dikes at the edge of the experimental marsh. Alternatively, model calculations may underestimate the water volume entering the marsh, possibly because of turbulence and heterogeneity in flow velocity profiles. However, the high bromide recovery relative to known amount of tracer release (115%) indicates instead a 15% overestimation of the T_0 ebb water volume. A reduction of the T_0 ebb by 15% would indeed result in an almost closed T_0 water budget, the balance between import and export being only 1.6% rather than the 18.9% reported in Table 1. Whatever the reason, the above-mentioned factors illustrate the shortcomings of traditional mass-balance studies.

Large errors in our conventional mass-balance budget did not allow for reliable whole-system N-transformation estimates. Although the water budget is also used in the calculations of the ^{15}N mass-balance budget, experimental errors in water estimates are of less consequence, because a known amount of tracer is added (import), and only the export relies on the water volume estimates. Thus, the 15% error (overestimation) in the water budget (T_0) indicated by the bromide data and discussed above results in a 15% error in the ^{15}N budget estimates. The clear observations that $^{15}NH_4^+$ is nitrified and that marsh surfaces are key sites for nitrification as well as nitrogen accumulation highlight the strengths of the whole-ecosystem ^{15}N labeling approach.

The ^{15}N mass-balance calculations revealed that, surprisingly, only a relatively small fraction of the added label was retained within the marsh. Uptake into the various marsh compartments is beyond the scope of this article and is discussed elsewhere (Gribsholt et al. unpubl. data), but collectively, sediment, roots, plants, and plant litter retained only ~4%, corresponding to 13% of the ^{15}N transformed (i.e., not exported as $^{15}NH_4^+$). Uptake by suspended algae and bacteria was limited (<2% of transformed ^{15}N), while nitrate was the largest single pool, accounting for 9% of the added tracer or 30% of the transformed ^{15}N. Nitrification has also been demonstrated to rival assimilative uptake of NH_4^+ in forested streams (e.g., Mulholland et al. 2000; Hamilton et al. 2001;

Peterson et al. 2001). Overall, our study shows that the marsh is quite important for N transformation, with almost one-third of the $^{15}NH_4^+$ added to floodwater transformed within the first tide. Assuming we overestimated the export of untransformed tracer by 15%, as indicated by the Br^- budget, the fraction of transformed ^{15}N was as high as 40%.

We were able to account for about 86% of the added ^{15}N and ascribe the missing 14% to either export as DON or denitrification to N_2. Detailed process studies summarized by Berman and Bronk (2003) have shown that ^{15}N uptake by microbes can result in rapid formation of ^{15}N-enriched DON. Moreover, uptake of ^{15}N by macrophytes and subsequent leaching of leaves may also result in ^{15}N enrichment of DON. However, methodological restrictions prevent us from evaluating the significance of DON. Although water–air fluxes were insignificant, gas emission during emersion (sediment–air flux) of $^{15}N_2O$ and $^{15}N_2$ produced by sedimentary nitrification and denitrification may also account for some loss. Furthermore, we recognize that several omitted compartments may represent minor losses as well. For instance, benthic and pelagic faunal components were omitted as a result of very low abundances.

To successfully trace the ^{15}N and construct a reliable budget for the entire marsh ecosystem, a prerequisite is an even distribution of tracer through the entire study area. For this purpose, we constructed a simple tracer addition device that allowed us to add tracer to the floodwater at a rate approximately proportional to the water volume. Simultaneous addition of the conservative tracer Br^- allowed us to confirm that a relatively even distribution was indeed obtained. Too much tracer solution was, however, added directly around the turn of the tide, resulting in Br^- concentrations twice as high as those observed in the main tide, and this was also reflected in a peak in excess concentrations of $^{15}NH_4^+$, $^{15}NO_3^-$, and ^{15}N-SPM. Since the last body of water entering the study site is also the first to exit, we believe this overlabeling to be of little consequence for the overall labeling and N processing within the study site and therefore for the interpretation of the results. This perception is corroborated by the relatively even Br^- concentrations recovered in the marsh water traps, indicating that we successfully obtained an even tracer distribution. On average, the added tracer increased the ^{15}N content to 1.3% of the ammonium pool and increased the total NH_4^+ concentration by approximately 14%. Nutrient concentration variability during flood tide (Fig. 3), however, resulted in a higher initial degree of labeling compared to the main tide. This initial period accounted for only a minor part of the total water volume, and therefore, we consider this of little significance. The added tracer probably did not accelerate in situ rates but merely substituted for in situ N species.

In this study the ^{15}N tracer was added in a short pulse (1.5 h) as opposed to the long-term (up to 6 weeks) continuous tracer addition approach adopted in previous ^{15}N whole-ecosystem tracer studies (e.g., Mulholland et al. 2000; Tobias et al. 2003; Ashkenas et al. 2004). The constraint of periodic, two-directional water flows in the tidal marsh and the complete drainage between tides renders a longer addition unfeasible. The short pulse labeling is, however, adequate for tracing the short–time scale processes such as nitrification. We added ^{15}N in the form of NH_4^+ primarily because ammonium is preferred over nitrate by most macrophytes as well as microphytes. Thus, a higher turnover of ammonium rather than nitrate would be expected. Also, nitrate concentrations in the Scheldt are much higher than those of ammonium, and ^{15}N enrichment of the NO_3^- pool would require a large addition of ^{15}N-NO_3^-, with high related costs.

Nitrification and the importance of the marsh surface area—Nitrate was quantitatively the most important fate for ^{15}N in our study, with nitrification accounting for 30% of the ^{15}N transformation. The validity of this mass-balance estimate is strongly supported by the estimate of the relative importance of nitrification (24%) based on the straightforward relation during T_0 ebb between the observed decrease and increase in excess $^{15}NH_4^+$ and $^{15}NO_3^-$ concentrations, respectively. Nitrification has also been reported to account for a substantial fraction (up to 50%) of the total $^{15}NH_4^+$ removal in in situ ^{15}N tracer studies of forested streams (Hamilton et al. 2001; Merriam et al. 2002; Ashkenas et al. 2004).

The occurrence of nitrification in the marsh is evident in several ways and is most clearly evident in the direct transfer of ^{15}N from the added ammonium pool to the nitrate pool, as seen in the increase in $\Delta\delta^{15}NO_3^-$ (Fig. 6b). Although the pelagic ammonium pool was only isotopically enriched during T_0, enriched nitrate was also exported in the following tides. This indicates that the marsh acts as at least a temporary sink for N, either through pore-water DIN exchange, sorption, or rapid assimilation by benthic microbes and subsequent mineralization. The very high $^{15}NO_3^- : Br^-$ ratios observed, especially during T_1, indicate a biological mechanism (microbial uptake and subsequently remineralization by nitrifiers) rather than physicochemical sorption as the main sink.

The significantly higher (four to nine times) nitrification rates observed on a whole-ecosystem scale (ENR) compared to the water column alone (WNR) clearly demonstrate that even in this nutrient-rich system, the large reactive surface area of sediments and biofilms in the marsh are the key sites for nitrification. Three factors may potentially be important controls on nitrification in the marsh ecosystem: nitrifier biomass, oxygen dynamics, and ammonium availability for nitrifiers. The distribution, abundance, and activity of nitrifiers is known to be influenced by their attachment to particles (Prosser 1989), and the surfaces of the dense vegetation and plant litter in the marsh may provide an excellent substratum for microbial colonization, just as epiphytic communities on submersed macrophytes have been demonstrated to be a major source of nitrification in nutrient-rich aquatic environments (Eriksson and Weisner 1999). Several authors have argued that establishment of macrophyte beds, a conspicuous, defining feature of the tidal marsh, should shift the location of greatest algal and bacterial growth from the water column and sediment to benthic plant surfaces because of the multiple advantages associated with an epiphytic biofilm habitat (e.g., Wetzel and Søndergaard 1998). Benthic nitrification may, however, also be enhanced as oxygen-releasing roots of marsh plants provide oxic subsurface microniches in otherwise anoxic sediments in which ammonium-oxidizing bacteria may thrive (Bodelier et al. 1996; Gribsholt and

Kristensen 2002). Nitrifying bacteria can survive as viable inactive cells during periods of low substrate concentrations or poor growing conditions such as low [O_2] (e.g., Verhagen et al. 1992; Bodelier et al. 1996) and can react instantaneously to favorable conditions. Although hypoxic conditions prevailed, O_2 exchange is rapid in the shallow, turbulent water, and O_2 was never fully depleted. The rapid response of the nitrifying population to inundation indicates adaptation to the specific environmental conditions in the tidal freshwater marsh. Because of the relatively high N availability in the floodwater, plant and heterotrophic bacteria competition for NH_4^+ becomes low enough to allow nitrifiers to flourish. Some ammonium limitation may occur, though, as at least WNR was correlated with ammonium concentrations. The importance of the marsh surface in N transformation is even evident from the intriguing temporal patterns in nutrient loadings observed in all tides. Only around the turn of the tides (maximum tide) did the [NH_4^+] equal that of the main river, while [NO_3^-] even exceeded it approximately halfway through flood as well as ebb tides. These large differences between floodwater and Scheldt water nutrient loading can be explained by the long distance over marsh creeks and surfaces through which the water travels before arriving at the study site and by the influence (uptake as well as transformation) this estuarine environment has already exerted on the water. The body of water initially entering the study site appears to experience the most contact with the sediments and biofilms, and thus the nitrifying (and denitrifying) microorganisms associated with it. Correspondingly, the pattern of decreasing [NH_4^+] and increasing [NO_3^-] in the first part of the ebb clearly shows that ammonium is being oxidized to nitrate within our study site while inundated. During the seepage phase, however, low and decreasing [DIN] could indicate N removal through temporary assimilation and denitrification.

Between tides, water continued to trickle out of our study site. The long distance to the main river, however, meant that although the water had left the study site, not all water left the marsh before the next flood. Some water remained in the marsh creek system and was pushed back into the study site with the next tide, as is evident from the elevated bromide concentration in the initial T_1-T_5 samples. While residing within the marsh, this water had been in intimate contact with the reactive marsh surface sediment, and N removal was very evident, as all initial floodwater samples were extremely depleted in DIN relative to the river water.

Denitrification—Denitrification is often considered the most important ultimate nitrogen removal pathway from marshes and other aquatic systems and has thus attracted much attention. On ecosystem scales, the importance of denitrification has most often been inferred from mass-balance studies, as the 'missing part' and is generally reported responsible for most nitrogen retention in freshwater ecosystems. Unfortunately, denitrification was not completely covered by our measurements. A small increase (2‰) in the isotopic ratio of N_2, however, as well as the temporal DIN concentration dynamics, indicate that denitrification occurs, especially during the seepage phase. During low tide, topographic and hydraulic gradients along creek banks can lead to drainage of marsh pore water into the creek; thus, the seepage water consists of a mixture of surface water trapped in depressions and between vegetation and pore water. Thus, this water has been in intimate contact with sediments and biofilms, where oxic and anoxic microniches may support high rates of coupled nitrification–denitrification.

No significant labeling of the N_2 pool was observed during the main tides. The lack of $^{15}N_2$ accumulation, however, does not exclude the possibility that denitrification took place. First, ^{15}N was added as ammonium, and the relatively short duration of the tide (~3 h) may not be sufficient for the transfer of ^{15}N via nitrification and denitrification to N_2 to occur at a sufficient rate for detection, even with a tight coupling between nitrification–denitrification. Second, the NO_3^- formed (~0.15 μmol L^{-1}) was diluted in the very high background [NO_3^-] (~350 μmol L^{-1}), and $^{15}N_2$ derived from the labeled NO_3^- pool ($\Delta\delta^{15}N$, Fig. 5) is therefore rather low. Third, since denitrification occurs mainly, perhaps even only, in the sediment, and the $\delta^{15}NO_3^-$ of pore water may not have been enriched significantly (because it is derived mainly from sedimentary ammonification and nitrification), it is likely that N_2 produced was not isotopically enriched. Fourth, part of the N_2 produced may have escaped to the atmosphere.

Besides being an end product of denitrification, the $^{15}N_2$ recovered during seepage could theoretically also be produced by anaerobic ammonium oxidation coupled to nitrate reduction (anammox) ($^{15}NH_4^+ + NO_2^- \rightarrow {}^{15}N_2 + 2\,H_2O$) (Van de Graaf et al. 1995). However, sediment incubations (performed according to Thamdrup and Dalsgaard 2002) in 2003 revealed that anammox is not an important process in this tidal freshwater marsh. Whole-core incubation of marsh sediment, on the other hand, revealed high denitrification rates (~0.5 mmol m^{-2} h^{-1}) in May 2003 (Gribsholt unpubl. data), similar to those reported for a nearby tidal freshwater marsh by Verhoeven et al. (2001) and in the Scheldt estuary by Middelburg et al. (1995), and much higher than those reported for more oligohaline North American freshwater marshes. More work is needed to determine the spatial and temporal patterns of denitrification and its importance for N-transformation in tidal freshwater marshes.

N_2O formation—Coinciding with the increase in $^{15}NO_3^-$ during T_0, we observed a clear increase in ^{15}N-labeled dissolved N_2O. Nitrous oxide is produced by three microbial processes: nitrification, denitrification, and dissimilatory reduction of nitrate to ammonia (Seitzinger 1988). While the importance and mechanism for N_2O production by denitrification are relatively well understood, our appreciation of the importance of nitrification for the global N_2O budget is still limited. The concurrent increase in $^{15}N_2O$ and $^{15}NO_3^-$ after addition of labeled ammonium observed in our study strongly indicates that the observed $^{15}N_2O$ production is largely due to nitrification. Thus, during T_0 excess $^{15}N_2O$ is directly correlated with excess $^{15}NO_3^-$ concentrations ($r^2 = 0.80$, $p < 0.05$). Moreover, the maximum $\Delta\delta^{15}N$ of N_2O is higher than that of NO_3^-, indicating that it comes directly from ammonium. This conclusion is further corroborated by the observed hypoxic conditions during large parts of all tides, as concentrations of O_2 have been clearly recognized

as the key control on N_2O production by both nitrification and denitrification, especially during high nutrient availability (e.g., Goreau et al. 1980; Jørgensen et al. 1984; de Bie et al. 2002).

During nitrification, oxidation of NH_4^+ has been shown to produce a $NO_3^-:N_2O$ ratio between 10:1 and 300:1 (Cole and Caraco 2001). Although largely produced by nitrification, the observed marsh N_2O production rate was quite low, and the $NO_3^-:N_2O$ ratio (663:1 to 1,441:1) is high compared to previous estimates based on studies with isolates. Middelburg et al. (1995) reported sediment–air N_2O fluxes and nitrification rates in tidal sediments along the Scheldt estuary corresponding to $NO_3^-:N_2O$ ratios of 278 to 3,333. Our whole-system estimates include not only the production but also the consumption of N_2O and NO_3^-. Since most nitrification occurs in the sediment, a large portion of the produced N_2O is most likely immediately consumed by denitrifying bacteria in the sediment, and thus never reaches the water phase.

Globally, human alterations of the nitrogen cycle have increased concentrations of the potent greenhouse gas N_2O (Vitousek et al. 1997), and while the increasing concentration of N_2O is clearly documented, the source of that increase remains a matter of some discussion. Most likely, many anthropogenic sources contribute (Vitousek et al. 1997), and although not quantified in this study, our results indicate that nitrification in wetlands receiving hypoxic, nutrient-rich water may contribute as well. While the importance of nitrification as a source of nitrous oxide triggered by low oxygen concentrations (in conjunction with high ammonium availability) has previously been shown on the estuarine scale (Barnes and Owens 1998; de Bie et al. 2002; Punshon and Moore 2004), this is, to our knowledge, the first study specific to tidal marsh ecosystems.

Marshes and the Scheldt estuary—To determine the role of tidal–freshwater–marsh nitrification to the nitrogen budget of the Scheldt estuary, we scaled our estimates of nitrification rates in our study site during water cover to the total area of fringing tidal freshwater marshes in the estuary. Estimates are based on the T_0 nutrient and water balances and T_0 nitrification rates (1.0–2.4 mmol m^{-2} h^{-1}) and a yearly inundation period of our study site of 691 h yr^{-1} (based on topography and mean tidal height at Tielrode [2002]). Annually, 36–81 kg N is nitrified in our study site, corresponding to 1,030–2,340 kg in the ~100,000 m^2 Tielrode marsh. Consequently, ~46,000–105,000 kg of riverborne ammonium will be nitrified yearly in the 4.5 km^2 of freshwater marshes fringing the Scheldt, equaling ~1.5–3.5% of the yearly ammonium load to the Scheldt (~3,000,000 kg yr^{-1}, Struyf et al. 2004). Variation in duration of water cover and reactive surface area (sediment, plant stems, litter) due to differences in topography and variations in heterotrophic activity due to nutrient availability and season will determine the processing of N. Therefore, extrapolation from our spring/early summer experiment with relatively high temperatures may overestimate annual nitrification. Water residence time and inundation frequency, however, are longer in large parts of the marsh compared to our study site; thus, our extrapolation to the entire Tielrode marsh may underestimate nitrification. In spite of these limitations, our extrapolations are reasonable because the relative large study area, covering all relevant vegetation types, is a good representative of freshwater marshes along the river. Overall, our results, in combination with those of other studies throughout the estuary, reveal that tidal freshwater marshes contribute little to the overall N-cycling of the Scheldt estuary, which is mainly governed by main-stream water column processes. This is likely due to a combination of the small surface of marshes relative to the overall surface of the estuary, very high nutrient loading, and short water residence time. However, if the large areas of brackish marshes in the Scheldt estuary (~20 km^2) transform NH_4^+ at comparable rates to our freshwater marsh site, as much as 252,000–573,000 kg, or 8.4–19.1% of the yearly ammonium load to the Scheldt, is potentially nitrified in tidal marshes.

References

ASHKENAS, L. R., S. L. JOHNSON, S. V. GREGORY, J. L. TANK, AND W. M. WOLLHEIM. 2004. A stable isotope tracer study of nitrogen uptake and transformation in a old-growth forest stream. Ecology **86:** 1725–1739.

BARNES, J., AND N. J. P. OWENS. 1998. Denitrification and nitrous oxide concentrations in the Humber Estuary, UK, and adjacent coastal zones. Mar. Pollut. Bull. **37:** 247–260.

BERMAN, T., AND D. A. BRONK. 2003. Dissolved organic nitrogen: A dynamic participant in aquatic ecosystems. Aquat. Microb. Ecol. **31:** 279–305.

DE BIE, M. J. M., J. J. MIDDELBURG, M. STARINK, AND H. J. LAANBROEK. 2002. Factors controlling nitrous oxide at the microbial community and estuarine scale. Mar. Ecol. Prog. Ser. **240:** 1–9.

BILLEN, G., C. LANCELOT, AND M. MEYBECK. 1991. N, P, and Si retention along the aquatic continuum from land to ocean, p. 19–44 *In* F. C. A. Mantoura, J-M. Martin, and R. Wollast [eds.], Ocean margin processes in global change. Wiley.

BODELIER, P. L. E., J. A. LIBOCHANT, C.W.P.M. BLOM, AND H. J. LAANBROEK. 1996. Dynamics of nitrification and denitrification in root-oxygenated sediments and adaptation of ammonia-oxidizing bacteria to low-oxygen or anoxic habitats. Appl. Environ. Microbiol. **62:** 4100–4107.

BORGES, A. V., B. DELILLE, L-S. SCHIETTECATTE, F. GAZEAU, G. G. ABRIL, AND M. FRANKIGNOULLE. 2004. Gas transfer velocities of CO_2 in three European estuaries (Randers Fjord, Scheldt, and Thames). Limnol. Oceanogr. **49:** 1630–1641.

BOWDEN, W. B. 1987. The biogeochemistry of nitrogen in freshwater wetlands. Biogeochemistry **4:** 313–348.

CAI, W., W. J. WIEBE, Y. WANG, AND J. E. SHELDON. 2000. Intertidal marsh as a source of dissolved inorganic carbon and a sink of nitrate in the Satilla river-estuarine complex in the southeastern U.S. Limnol. Oceanogr. **45:** 1743–1752.

DAME, R., AND OTHERS. 1996. The outwelling hypothesis and North Inlet, South Carolina. Mar. Ecol. Prog. Ser. **33:** 217–229.

DESENDER, K., AND J. P. MAELFAIT. 1999. Diversity and conservation of terrestrial arthropods in tidal marshes along the River Schelde: A gradient analysis. Biol. Conserv. **87:** 221–229.

ERIKSSON, P. G., AND S. E. B. WEISNER. 1999. An experimental study on effects of submersed macrophytes on nitrification and denitrification in ammonium-rich aquatic systems. Limnol. Oceanogr. **44:** 1993–1999.

GOREAU, T. J., W. A. KAPLAN, S. C. WOFSY, M. B. MCELROY, F. W. VALOIS, AND S. W. WATSON. 1980. Production of NO_2^- and

N_2O by nitrifying bacteria at reduced concentration of oxygen. Appl. Environ. Microbiol. **40:** 526–532.

GRIBSHOLT, B., AND E. KRISTENSEN. 2002. Effects of bioturbation and plant roots on salt marsh biogeochemistry: A mesocosm study. Mar. Ecol. Prog. Ser. **241:** 71–87.

HAMILTON, S. K., J. L. TANK, D. F. RAIKOW, W. M. WOLLHEIM, B. J. PETERSON, AND J. R. WEBSTER. 2001. Nitrogen uptake and transformation in a midwestern U.S. stream: A stable isotope enrichment study. Biogeochemistry **54:** 297–340.

HOLMES, R. M., J. W. MCCLELLAND, D. M. SIGMAN, B. FRY, AND B. J. PETERSON. 1998. Measuring $^{15}N\text{-}NH_4^+$ in marine, estuarine and fresh waters: An adaptation of the ammonium diffusion method for samples with low ammonium concentrations. Mar. Chem. **60:** 235–243.

———, B. J. PETERSON, L. A. DEEGAN, J. E. HUGHES, AND B. FRY. 2000. Nitrogen biogeochemistry in the oligohaline zone of a New England estuary. Ecology **81:** 416–432.

HORRIGAN, S. G., J. P. MONTOYA, J. L. NEVINS, J. J. MCCARTHY, H. DUCKLOW, R. GOERICKE, AND T. MALONE. 1990. Nitrogenous nutrient transformations in the spring and fall in the Chesapeake Bay. Estuar. Coastal Shelf Sci. **30:** 369–391.

HOWARTH, R. W., AND OTHERS. 1996. Regional nitrogen budgets and riverine N & P fluxes for the drainages to the North Atlantic Ocean: Natural and human influences. Biogeochemistry **35:** 75–139.

HUGHES, J. E., L. A. DEEGAN, B. J. PETERSON, R. M. HOLMES, AND B. FRY. 2000. Nitrogen flow through the food web in the oligohaline zone of a New England estuary. Ecology **81:** 433–452.

JØRGENSEN, K. S., H. B. JENSEN, AND J. SØRENSEN. 1984. Nitrous oxide production from nitrification and denitrification in marine sediment at low oxygen concentration. Can. J. Microbiol. **30:** 1073–1078.

KLING, G. W. 1994. Ecosystem-scale experiments. The use of stable isotopes in fresh waters, p. 91-120. *In* L. A. Baker [ed.], Environmental chemistry of lakes and reservoirs. American Chemical Society.

MERRIAM, J. L., W. H. MCDOWELL, J. L. TANK, W. M. WOLLHEIM, C. L. CRENSHAW, AND S. L. JOHNSON. 2002. Characterizing nitrogen dynamics, retention and transport in a tropical rainforest stream using an in situ ^{15}N addition. Freshw. Biol. **47:** 143–160.

MERRILL, J. Z., AND J. CORNWELL. 2000. The role of oligohaline marshes in estuarine nutrient cycling, p. 425–441. *In* M. P. Weinstein and D. A. Kreeger [eds.], Concepts and controversies in tidal marsh ecology. Kluwer.

MIDDELBURG, J. J., G. KLAVER, J. NIEUWENHUIZE, R. M. MARKUSSE, T. VLUG, AND J.F.W.A. VAN DER NAT. 1995. Nitrous oxide emission from estuarine intertidal sediments. Hydrobiologia **311:** 43–55.

———, AND J. NIEUWENHUIZE. 2000. Uptake of dissolved inorganic nitrogen in turbid, tidal estuaries. Mar. Ecol. Prog. Ser. **192:** 79–88.

MULHOLLAND, P. J., J. L. TANK, D. M. SANZONE, W. M. WOLLHEIM, B. J. PETERSON, J. R. WEBSTER, AND J. L. MEYER. 2000. Nitrogen cycling in a forest stream determined by a ^{15}N tracer addition. Ecol. Monogr. **70:** 471–493.

NIEUWENHUIZE, J., Y. E. M. MAAS, AND J. J. MIDDELBURG. 1994. Rapid analysis of organic carbon and nitrogen in particulate materials. Mar. Chem. **45:** 217–224.

PETERSON, B. J., M. BAHR, AND G. W. KLING. 1997. A tracer investigation of nitrogen cycling in a pristine tundra river. Can. J. Fish. Aquat. Sci. **54:** 2361–2367.

———, AND OTHERS. 2001. Control of nitrogen export from watersheds by headwater streams. Science **292:** 86–90.

PUNSHON, S., AND R. M. MOORE. 2004. Nitrous oxide production and consumption in a eutrophic coastal embayment. Mar. Chem. **91:** 37–51.

SCHINDLER, D. W. 1998. Replication versus realism: The need for ecosystem-scale experiments. Ecosystems **1:** 323–334.

SEITZINGER, S. P. 1988. Denitrification in freshwater and coastal marine ecosystems: Ecological and geochemical significance. Limnol. Oceanogr. **33:** 702–724.

SIGMAN, D. M., M. A. ALTABET, R. MICHENER, D. C. MCCORKLE, B. FRY, AND R. M. HOLMES. 1997. Natural abundance-level measurement of the nitrogen isotopic composition of oceanic nitrate: An adaptation of the ammonia diffusion method. Mar. Chem. **57:** 227–242.

SOETAERT, K., P. M. J. HERMAN. 1995. Nitrogen dynamics in the Westerschelde estuary (SW Netherlands) estimated by means of the ecosystem model MOSES. Hydrobiologia **311:** 225–246.

———, J. J. MIDDELBURG, C. HEIP, P. MEIRE, S. VAN DAMME, T. MARIS. In press. Long-term change in dissolved inorganic nutrients in the heterotrophic Scheldt estuary (Belgium, The Netherlands). Limnol. Oceanogr.

STRUYF, E., S. VAN DAMME, AND P. MEIRE. 2004. Possible effects of climate change on estuarine nutrient fluxes: A case study in the highly nutrified Schelde estuary (Belgium, The Netherlands). Estuar. Coastal Shelf Sci. **60:** 649–661.

TANK, J. L., AND OTHERS. 2000. Analysis of nitrogen cycling in a forest stream during autumn using a ^{15}N-tracer addition. Limnol. Oceanogr. **45:** 1013–1029.

THAMDRUP, B., AND T. DALSGAARD. 2002. Production of N_2 through anaerobic ammonium oxidation coupled to nitrate reduction in marine sediments. Appl. Environ. Microbiol. **68:** 1312–1318.

TOBIAS, C. R., M. CIERI, B. J. PETERSON, L. A. DEEGAN, J. VALLINO, AND J. E. HUGHES. 2003. Processing watershed-derived nitrogen in a well-flushed New England estuary. Limnol. Oceanogr. **48:** 1766–1778.

———, S. A. MACKO, I. C. ANDERSON, E. A. CANUEL, AND J. W. HARVEY. 2001. Tracking the fate of a high concentration groundwater nitrate plume through a fringing marsh: A combined groundwater tracer and an in situ isotope enrichment study. Limnol. Oceanogr. **46:** 1977–1989.

VAN DE GRAAF, A. A., A. MULDER, P. DE BRUIJN, M. S. M. JETTEN, L. A. ROBERTSON, AND J. G. KUENEN. 1995. Anaerobic oxidation of ammonium is a biologically mediated process. Appl. Environ. Microbiol. **61:** 1246–1251.

VERHAGEN, F. J. M., H. DUYTS, AND H. J. LAANBROEK. 1992. Competition for ammonium between nitrifying and heterotrophic bacteria in continuously percolated soil columns. Appl. Environ. Microbiol. **58:** 3303–3311.

VERHOEVEN, J. T. A., D. F. WHIGHAM, R. VAN LOGTESTIJN, AND J. O'NEILL. 2001. A comparative study of nitrogen and phosphorous cycling in tidal and non-tidal riverine wetlands. Wetlands **21:** 210–222.

VITOUSEK, P. M., AND OTHERS. 1997. Human alterations of the global nitrogen cycle: Sources and consequences. Ecol. Appl. **7:** 737–750.

WEISS, R. F., AND B. A. PRICE. 1980. Nitrous oxide solubility in water and seawater. Mar. Chem. **8:** 347–359.

WETZEL, R. G., AND M. SØNDERGAARD. 1998. Role of submerged macrophytes for the microbial community and dynamics of dissolved organic carbon in aquatic ecosystems, p. 133–148. *In* E. Jeppesen, M. Søndergaard, M. SØNDERGAARD, AND K. CHRISTOFFERSEN [EDS.], The structuring role of submerged macrophytes in lakes. Springer.

WOLLHEIM, W. M., AND OTHERS. 2001. Influence of stream size on ammonium and suspended particulate nitrogen processing. Limnol. Oceanogr. **46:** 1–13.

Received: 1 December 2004
Accepted: 6 June 2005
Amended: 6 July 2005